Explicitly filtered large eddy simulation on unstructured grids

By S. T. Bose, P. Moin AND F. Ham

1. Motivation and objectives

There is growing interest in the use of large-eddy simulation (LES) for engineering design in conjunction with or in lieu of traditional RANS solvers. Because of the complex geometries prevalent in practical configurations, unstructured grid based solvers are frequently utilized. In order to further the predictive capabilities of unstructured grid based LES solvers, it is necessary to provide accurate subgrid stress (SGS) models and additionally, implement mechanisms to isolate the effect of discretization errors from errors induced by the closure models. Previous simulations have demonstrated that solution of the explicitly filtered LES governing equations can yield turbulent statistics that are independent of the underlying grid (Bose *et al.* 2010). This allows for a true assessment of the accuracy of the SGS model in the absence of discretization errors. However, previous work has limited the use of explicit filtering to structured grids. Discretization errors are usually more severe in unstructured grid solvers than in their structured grid counterparts, and thus, there is a need to extend the explicit filtering methodology to unstructured solvers.

Predictive engineering simulations also require quantification of aleatoric uncertainties arising from the natural variability of physical parameters. Non-intrusive algorithms to evaluate these uncertainties require a large number of simulations to characterize the effects of the parameter changes. Due to the large number of simulations needed, coarse resolutions may be required for practical large-eddy simulations. As a result, there will be a greater emphasis on the accuracy of SGS models. Finely resolved LES that approach resolutions used for direct numerical simulations are commonplace, especially in simulations of wall-bounded flows. It is unlikely that these finely resolved studies will elucidate the deficiencies that exist in SGS models. Mixed models (e.g., scale similarity model of Bardina *et al.* 1984; gradient model of Clark *et al.* 1979) have been shown to be more accurate than SGS models that are purely based on a gradient-diffusion hypothesis (Vreman *et al.* 1997; Meneveau & Katz 2000; Winckelmans *et al.* 2001). We have recently proposed a class of dynamic, mixed models that have been derived from the explicitly filtered LES governing equations (Bose & Moin 2010). These models predicted mean velocity profiles of high Reynolds number wall-bounded flows in very coarse simulations within a couple percent of DNS data. However, the implementation of mixed SGS models has been largely limited to structured grid solvers as well. The stability problems encountered by structured solvers when employing mixed models are often exacerbated by the numerical instabilities that arise from discretization on unstructured grids. A secondary objective of the current study is to implement the dynamic, mixed models suggested in Bose & Moin (2010) to an unstructured grid solver.

This brief details the implementation of the explicitly filtered governing equations and the mixed model into an unstructured solver (Section 2) and presents results of an ex-

plicitly filtered large-eddy simulation of a high Reynolds number rectangular duct flow (Section 3). Some concluding remarks and future directions are outlined in Section 4.

2. Explicitly filtered LES on unstructured grids

2.1. *Explicitly filtered LES*

Large-eddy simulation directly solves the dynamics of the large-scale, energy-containing motions in turbulent flows while modeling the effect of the unresolved scales on the resolved scales. Formally, the distinction between the resolved and unresolved scales is achieved through a filtering operator:

$$\bar{u}_i(x) = \int_\Omega G\left(x, x'; \Delta_f\right) u_i(x') dx', \tag{2.1}$$

where the filtered velocity field, $\bar{u}_i$, represents the resolved scales. The filtering operator (Eq. 2.1) is applied to the Navier-Stokes equation to derive the the governing equations for LES, written here in an explicitly filtered form:

$$\frac{\partial \bar{u}_i}{\partial t} + \frac{\partial \overline{\bar{u}_i \bar{u}_j}}{\partial x_j} = -\frac{\partial \bar{p}}{\partial x_i} + \frac{1}{Re}\frac{\partial^2 \bar{u}_i}{\partial x_j \partial x_j} - \frac{\partial \tau_{ij}}{\partial x_j}, \tag{2.2}$$

$$\tau_{ij} = \overline{u_i u_j} - \overline{\bar{u}_i \bar{u}_j}, \tag{2.3}$$

where τ_{ij} is the subgrid stress tensor resulting from the nonlinear interaction of the unresolved scales with the resolved scales. Eq. 2.2 differs from the traditional LES formulation as the Leonard stress is directly calculated and is subsumed into the convective term. For the present study, the dynamic mixed model suggested in Bose & Moin (2010) is used to model the SGS tensor:

$$\tau_{ij} = \overline{u'}_i \bar{u}_j + \bar{u}_i \overline{u'}_j + \overline{u'}_i \overline{u'}_j - 2Ck^* |\bar{S}|^{-1} \bar{S}_{ij}, \tag{2.4}$$

where $k^* = \frac{1}{2}\overline{u'}_k \overline{u'}_k$ and C is a dynamic, global coefficient (Bose & Moin 2010). The filtered unresolved velocity field, $\overline{u'}_i = \bar{u}_i - \bar{\bar{u}}_i$, is the exact projection of the unresolved velocity field into the range of the filter kernel. The construction of Eq. 2.4 restores Galilean invariance to the explicitly filtered LES governing equation in Eq. 2.2. Note that Eq. 2.4 is not mathematically equivalent to either the Bardina scale similarity model or the approximate deconvolution approach of Stolz *et al.* (2001). To date, simulations conducted with this SGS model for the explicitly filtered LES equations have been stable without the eddy viscosity term in Eq. 2.4 contrary to most prior experience with mixed models, although no formal proof of this stability exists.

2.2. *Differential filtering*

The explicitly filtered governing equation in Eq. 2.2 requires formal definition of the filter applied in order to evaluate the convective term. This poses a level of difficulty in an unstructured solver. The filtering approach on structured grids was to apply a tensor product of one-dimensional (1D) filters where the 1D filters were defined by a weighted sum of neighboring grid points. The filter width could be fixed when the grid was refined by expanding the 1D filtering stencil on the finer grids. A straightforward extension of this approach is obviously not possible on an unstructured grid because an obvious

dimensional splitting is not available. Marsden *et al.* (2002) and Haselbacher & Vasilyev (2003) have suggested the unstructured generalization of the structured grid approach where the filtering operator still relies on a weighted sum of neighboring values. The primary difficulty of both these approaches is that there is no way to ensure that the filtering operator is well behaved (i.e, $0 \leq \widehat{G}(k) \leq 1 \; \forall k$), and moreover, the exact behavior of the filter kernel is strongly controlled by the distribution of the surrounding mesh points. The algorithm of Marsden *et al.* (2002) additionally requires a careful selection of a subset of neighboring grid points, but it is not obvious that a reasonable subset of neighboring mesh points will exist in the presence of badly skewed and stretched grids. Another difficulty is that there is no clear way to fix the filter width in physical space when the grid is refined even if the data structures of the unstructured solvers are altered in order to allow for more neighbors. The alternative approach taken here is to specify a continuous filter kernel and subsequently discretize the filtering operation in Eq. 2.1. Due to the difficulties in discretizing the long-range effects of the filtering kernel, the filtering operator is implicitly defined through the solution of an elliptic relaxation equation (Germano 1986*a*,*b*):

$$\bar{\phi} - \frac{\partial}{\partial x_j}\left(p\frac{\partial \bar{\phi}}{\partial x_j}\right) = \phi, \tag{2.5}$$

where $p = p(x)$ is related to the filter width. Because the filter width is specified at the continuous level, it is agnostic to the underlying grid and therefore, decouples the filtering operator from the grid used. The operator in Eq. 2.5 is written in divergence form (which differs slightly from that suggested by Germano 1986*a*) to allow a finite volume discretization. This form has some additional properties that are discussed below. The generalized form of the differential filter has been studied in the context of adjoint filtering operators by Vreman (2004). The relationship between $p(x)$ and the filter width can be estimated by considering the case where p is constant in the domain. The filtering kernel for constant p on an unbounded domain is known (Germano 1986*b*):

$$G(x', x; p) = \frac{1}{4\pi p}\frac{\exp\left(-|x' - x|/\sqrt{p}\right)}{|x' - x|}, \tag{2.6}$$

and the singularity at $x' = x$ is integrable. It can be shown that as $p \to 0$, the filtering kernel approaches the Dirac delta function. By equating the second moment of the filter kernel in Eq. 2.6 with the second moment of a spherical top hat kernel with a radius of $\Delta_f/2$, the relationship between p and the filter width is $p = \Delta_f^2/40$. Figure 1 shows the result of applying the filtering operator on a grid with local grid refinement but a constant filter width parameter, p. The filtered solution does not show any artifacts from the local grid refinement and shows that the filtering procedure is robust on arbitrary polyhedra.

The only constraint that is placed on the filter width parameter, p, is that it vanishes at non-periodic boundaries. The fact that p vanishes makes the differential operator in Eq. 2.5 singular and therefore, no boundary conditions need to be specified. In one dimension, Eq. 2.5 is a singular Sturm-Liouville equation. Physically interpreted, the filter width should vanish at the wall because the filtered velocity field, $\bar{u}$, and unfiltered velocity field, u, utilize the same boundary conditions. Lastly, because p vanishes at boundaries, the total momentum of the velocity field is preserved by the filtering operation. This is shown by integrating Eq. 2.5 over the total domain and applying the

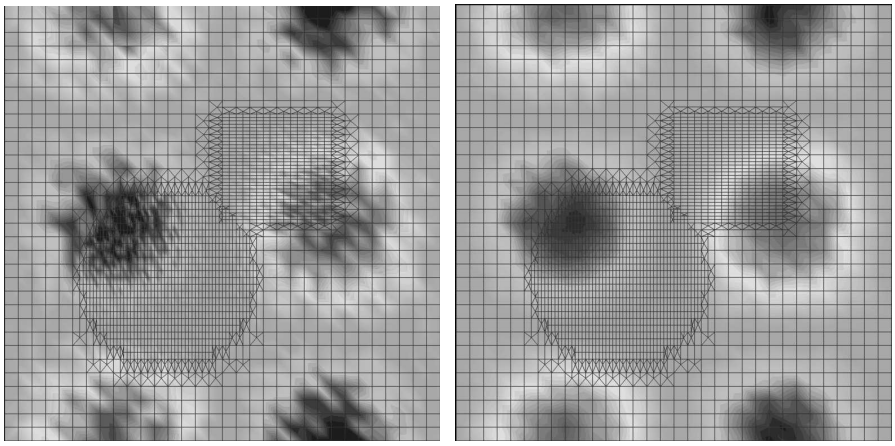

FIGURE 1. A sinusoidal function with superimposed random noise (20% amplitude) on an unstructured grid with two regions of local grid refinement unfiltered (left) and filtered (right).

divergence theorem. Although this filtering operator had been suggested much earlier and used in numerous mathematical analyses (Berselli *et al.* 2006), it has rarely been used for actual LES calculations. Mullen & Fischer (1999) utilized Eq. 2.5 with a constant p, but required specification of boundary conditions (e.g., no-slip for $\bar{u}$). The differential filtering approach detailed above was used by You *et al.* (2010) for the explicitly filtered compressible LES equations, and is implemented for the incompressible LES equations here.

2.3. *SGS model driven grid refinement*

One of the advantages of an unstructured grid based code is the ability to perform local grid refinement in regions of strong turbulent activity. For zero-equation SGS models for LES, there is insufficient information to dictate grid refinement because it is unclear how much energy is locally present at the subgrid scales. The current approach is to use the subgrid kinetic energy surrogate, $k^* = \frac{1}{2}\overline{u'}_k\overline{u'}_k$, to identify the regions where refinement is required. The filtered subgrid velocity field, $\overline{u'}_k$, is the linear extrapolation of the unresolved velocity field from the resolved field and thus, can be used to select regions where the true flow is under-resolved with respect to the filter width. Using the statistics of k^* from a coarse grid, a threshold for k^*_c is set and cells that exceed this threshold are refined. Figure 2 shows the mean values of k^* (averaged in time and in the homogeneous streamwise direction) in the yz plane for a turbulent duct flow, which is then used as a threshold for the refinement process. For a threshold of $\overline{u'}* = 0.03$, the local grid refinement increased the total number of cells by about six percent from the initial duct flow grid. The refinement is performed only in the spanwise direction because of the importance of the spanwise resolution in high Reynolds number wall-bounded flows. Unfortunately, the k^* criterion does not suggest the most efficient use of anisotropy in the grid refinement which has to be supplemented with physical intuition.

The grid refinement procedure outlined above can be done using either a fixed filter width or allowing for the filter width to reduce with the grid size, thereby resolving additional scales. The refinement used for the turbulent duct flow was a simultaneous grid and filter width reduction because of the coarseness of the initial mesh. In situations

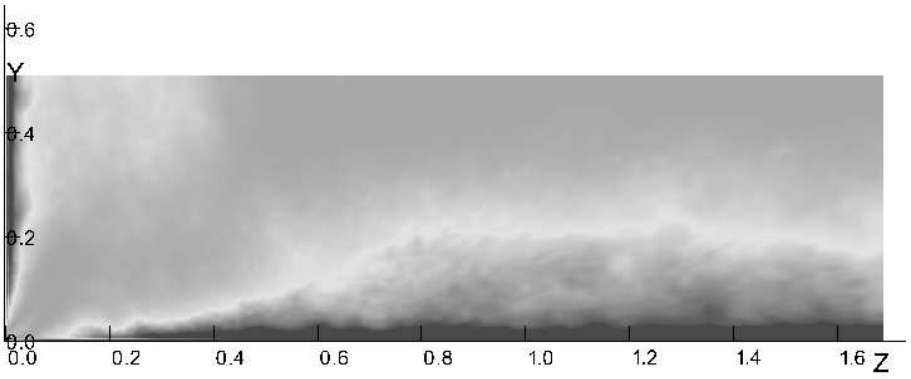

FIGURE 2. Mean contours (1×10^{-5} to 1×10^{-3}; log-scale) of k^* in the bottom left quadrant in a simulation of a rectangular duct flow. Cells that exceeded $u^* = 0.03$ were subsequently refined.

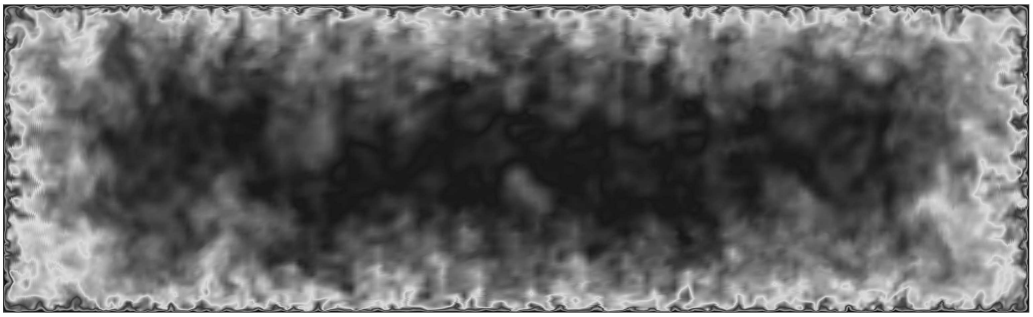

FIGURE 3. Instantaneous streamwise velocity in the yz plane in a rectangular duct with cross section of $3.33H \times H$; contour levels are from 0 to $1.4U_b$.

where the filter width is fixed and the grid is refined, the use of the k^* criteria is justified because it is likely that the influence of numerical errors will be most severe where the true solution of the Navier-Stokes equation is least resolved with respect to the filter width.

3. LES of an Re=50,000 rectangular duct flow

Explicitly filtered large-eddy simulation of a rectangular duct with an aspect ratio, $AR = W/H$, of 3.33 is performed. The Reynolds number, $Re = U_b H/\nu$, of the flow is $50,000$ where the Reynolds number is defined based on the bulk velocity and the height of the duct. The Reynolds number can also be defined with respect to the bulk velocity and the hydraulic diameter, which is $Re_{H_d} \approx 77000$ for this configuration. The LES is performed on a domain that measures $12H \times H \times 3.33H$. The aspect ratio of the duct can be seen in Figure 3, which shows contours of the instantaneous streamwise velocity in the yz plane. No-slip boundary conditions are applied on the four enclosing walls and periodic boundary conditions are applied along the streamwise direction. In the following discussion, the y coordinate denotes the direction normal to the bottom wall ($0 \leq y \leq H$) and the z coordinate denotes the direction normal to the side wall ($0 \leq z \leq 3.33H$). The final mesh used for the simulation consists of approximately 15

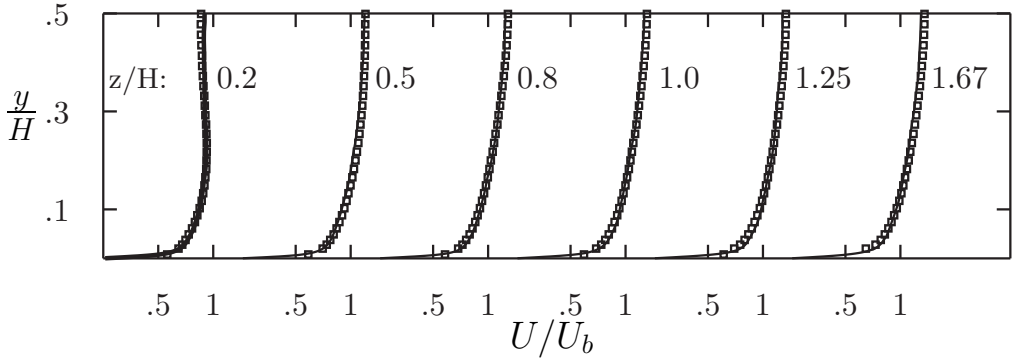

FIGURE 4. Mean streamwise velocity profiles at different spanwise locations for the explicitly filtered LES (solid lines) and the experimental measurements of Kolade (2010) (symbols).

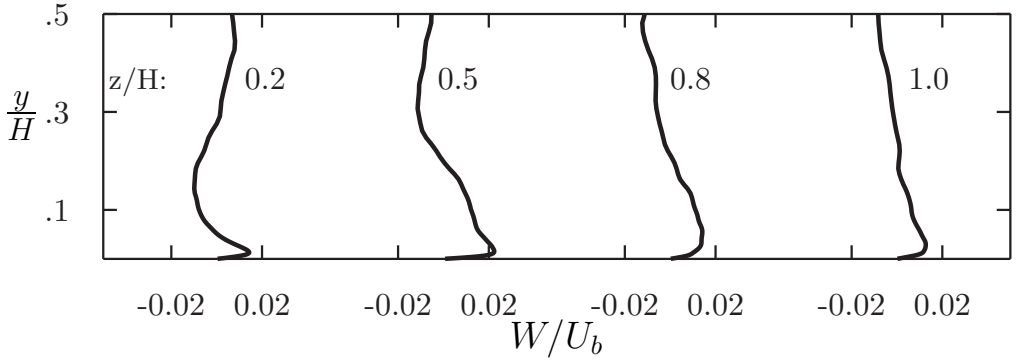

FIGURE 5. Mean spanwise velocity profiles at different spanwise locations for the explicitly filtered LES.

million control volumes, with approximately 3×10^4 hanging node elements that exist at two-to-one grid transitions that appear from the grid refinement procedure detailed above. Nominally, the local filter width is estimated to be 1.8 times the local grid size. A more rigorous estimate would require the solution of the Green's function corresponding to the differential operator in Eq. 2.5 at each grid point. Based on this estimate and the value of u_τ measured experimentally, the resolution of the LES is $\Delta x_f^+ \approx 160$, $\Delta y_f^+(\max) \approx 60$, and $\Delta z_f^+(\max) \approx 70$. The grid is stretched such that $\Delta y^+ \approx 1$ at the top and bottom walls and $\Delta z^+ \approx 1$ at the side walls. The simulation is chosen to be extremely coarse in order to highlight the deficiencies of the SGS model. The coarse resolution is close to that used by Bose & Moin (2010) for the simulation of an $Re_\tau = 2000$ channel flow that yielded acceptable predictions of the mean velocity profile.

Figure 4 shows the mean streamwise velocity profiles compared to the experimental measurements of Kolade (2010) at different spanwise locations. All of the velocity profiles presented are normalized with respect to the bulk velocity, U_b. Overall agreement with the experimental measurements is reasonable and the errors are within a few percent. Inflection in the streamwise mean velocity profiles is observed for spanwise locations closer to the side wall, $z/H < 0.5$. This is the likely signature of the secondary flow that develops in the corners of the rectangular duct. Figure 5 shows the mean spanwise velocity profiles at spanwise locations closer to the side wall. The magnitude of the mean spanwise velocity is about 2% of the bulk velocity, which is in qualitative agreement with other studies of corner flows in rectangular ducts (Gavrilakis 1992; Brundrett & Baines

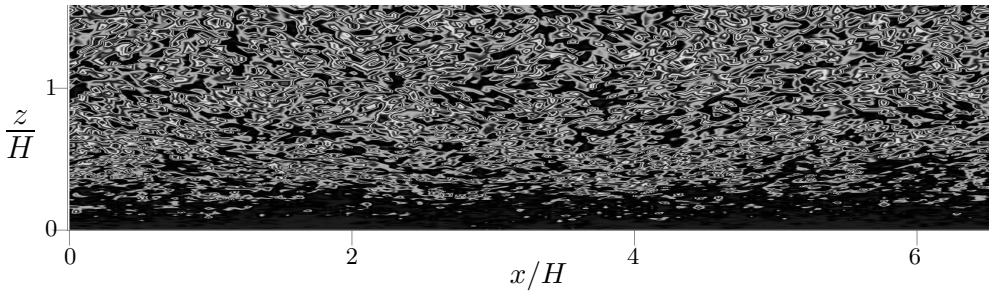

FIGURE 6. Instantaneous values of $|\tau^{od}| = \sqrt{\tau_{12}^2 + \tau_{13}^2 + \tau_{23}^2}$ in an $x - z$ plane at $y/H = 0.025$ (half of the duct span and half of the duct length shown). Contour levels are from $0, 0.05U_b^2$.

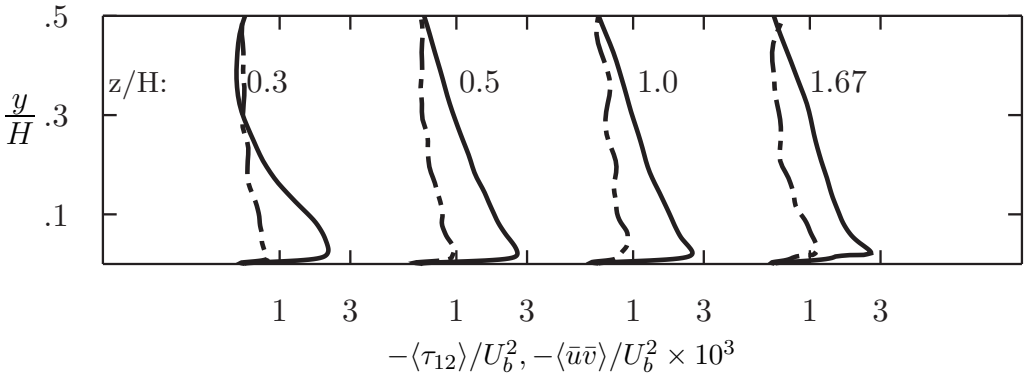

FIGURE 7. Mean profiles of the uv Reynolds shear stress decomposed into contributions from the resolved scales (———) and the SGS model (—·—) at different spanwise locations.

1964). Figure 6 shows the instantaneous magnitude of the off-diagonal components of the SGS tensor as defined in Eq. 2.4 in an x-z plane that is located $y/H = 0.025$ from the bottom wall of the duct. The instantaneous SGS stress is limited in the corner of the duct ($z/H = 0$ and 3.33), but appears more uniform in the region $0.75 < z/H < 2.58$. Figure 7 shows the mean total Reynolds shear stress, $\langle\bar{u}\bar{v} + \tau_{12}\rangle$, at different spanwise locations in the duct. The SGS contribution to the shear stress is greater than one third of the peak value achieved by the resolved scales away from the side walls indicating the importance of the SGS model in predicting the mean flow at spanwise locations $z/H \geq 0.5$. The SGS contribution is reduced, however, at $z/H = 0.3$, suggesting that flow is largely resolved in the vicinity of the sidewalls.

Figure 8 depicts the streamlines for the mean secondary flow in one quadrant of rectangular duct showing two pronounced vortices. Note that the secondary mean velocity near the spanwise midplane of the duct is very small, making the streamlines of the rightmost vortex susceptible to statistical convergence errors. The equation for the mean streamwise vorticity is given by (Durbin & Pettersson-Reif 2010)

$$V\frac{\partial\Omega_x}{\partial y} + W\frac{\partial\Omega_x}{\partial z} = \nu\left(\frac{\partial^2\Omega_x}{\partial y^2} + \frac{\partial^2\Omega_x}{\partial z^2}\right)$$
$$+\frac{\partial^2}{\partial y\partial z}\left(\langle v'^2\rangle - \langle w'^2\rangle\right) - \frac{\partial^2\overline{v'w'}}{\partial y^2} + \frac{\partial^2\overline{v'w'}}{\partial z^2}, \tag{3.1}$$

where $\langle\cdot\rangle$ denotes the averaging operator. It has been suggested that the anisotropy of the

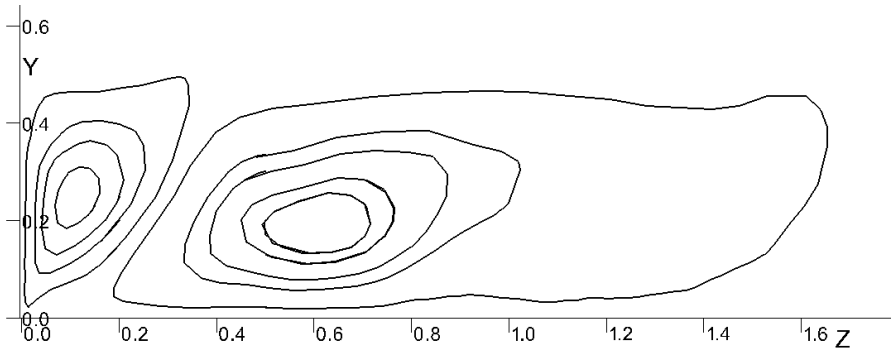

FIGURE 8. Streamlines of the secondary mean velocity vector, $\vec{U} = (0, V, W)$, in the bottom left quadrant of the yz plane in a rectangular duct with aspect ratio 3.33.

normal Reynolds stresses in Eq. 3.1 is responsible for the streamwise vorticity generation (Bradshaw 1987). The normal stress (anisotropy) can be decomposed into a resolved component and a SGS contribution

$$\langle v'^2 \rangle = \langle v^2 \rangle - \langle v \rangle^2 \approx \langle \bar{v}^2 \rangle - \langle \bar{v} \rangle^2 + \langle \tau_{22} \rangle, \tag{3.2}$$

and a similar decomposition exists for w'^2. The first two terms in the above expression represent the contribution from the resolved scales and the last term on the right is the SGS contribution to the normal Reynolds stress. Figure 9 shows the mean anisotropy measured in the normal stresses decomposed into its resolved and SGS components. Although the SGS contribution to the normal stress anisotropy does not dominate that contained in the resolved scales, it is still substantial, especially in the region $z/H = 0.5 - 0.8$. Thus, the dynamics of the rightmost secondary vortex that is centered at $z/H \approx 0.6$ (see Figure 8) is largely affected by the SGS model. Conversely, the SGS contribution to the normal stress anisotropy is much smaller closer to the sidewall ($z/H = 0.12, 0.20$), suggesting that the secondary vortex closer to the sidewall is driven mostly by the resolved scales. The decreased contribution from the SGS model to the normal stress anisotropy near the sidewall is consistent with the declining contribution of the SGS model to the Reynolds shear stress observed earlier, further implying that the flow in the region $z/H < 0.3$ is mostly resolved. The secondary Reynolds shear stress, $\overline{v'w'}$, that appears in Eq. 3.1 is of the same order of magnitude as the normal stress anisotropy, and so the above arguments regarding the importance of the subgrid scale model holds for the secondary Reynolds shear stress as well.

4. Concluding remarks and future work

The explicitly filtered framework and recently developed dynamic, mixed models have been implemented in an incompressible, unstructured grid solver. A coarse, explicitly filtered LES of a moderately high Reynolds number rectangular duct flow has been performed and good predictions of mean velocity profiles have been obtained. The contributions to the total Reynolds stress from the SGS model are substantial, especially in regions away from the side walls and therefore, the SGS model is integral to the predictions of the mean velocity profiles.

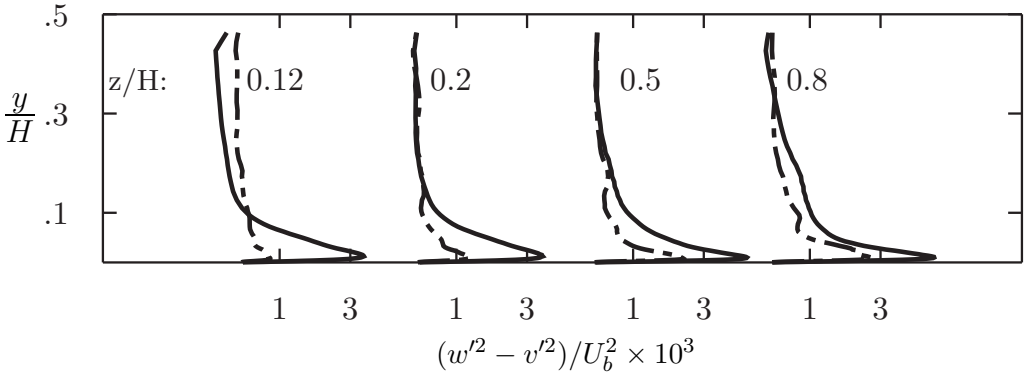

FIGURE 9. Mean profiles of the normal stress anisotropy, $(w'^2 - v'^2)/U_b^2$, decomposed into contributions from the resolved scales (———) and the SGS model (—·—) at different spanwise locations.

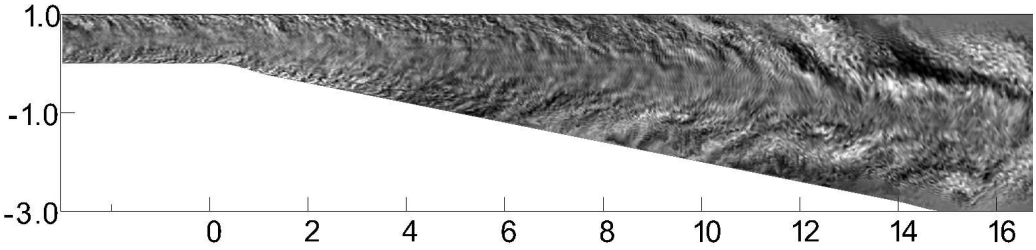

FIGURE 10. Instantaneous spanwise velocity from the LES of the 3D diffuser of Kolade (2010) at $z/H \approx 1.67$. Contours are from $-0.2U_b$ to $0.2U_b$.

Confined flows of engineering interest also routinely exhibit boundary layer separation. The dynamic mixed model proposed in Eq. 2.4 has now been studied in several simulations of high Reynolds number wall-bounded flows, but has not been evaluated in flows with boundary layer separation. The rectangular duct flow simulated in the present study is the inlet to the three-dimensional stalled diffuser (Kolade 2010). An explicitly filtered LES of the diffuser has been initiated and a slice through its midplane is shown in Figure 10. Both the bottom wall and the side wall of the duct deflect expanding the cross section to $4H \times 4H$ at the outlet. The importance of the SGS model and its ability to accurately predict the separation and reattachment of the boundary layer will be assessed.

Acknowledgments

This work has been supported by the Department of Energy Computational Science Graduate Fellowship under grant number DE-FG02-97ER25308 and through the Department of Energy PSAAP program. Computational resources provided at NERSC (Hopper) and LLNL (BlueGene/L) are gratefully acknowledged. Additional computational resources provided through an NSF MRI-2 grant (Certainty) are acknowledged.

REFERENCES

Bardina, J., Ferziger, J. H. & Reynolds, W. C. 1984 Improved turbulence models based on LES of homogeneous incompressible turbulent flows. *Tech. Rep.* TF-19. Dept, of Mech. Eng, Stanford Univ.

Berselli, L. C., Iliescu, T. & Layton, W. J. 2006 *Mathematics of large-eddy simulation of turbulent flows*. Springer.

Bose, S. T. & Moin, P. 2010 A class of dynamic mixed models for explicitly filtered LES. *Ctr. Turb. Res. Ann. Res. Briefs* pp. 223–236.

Bose, S. T., Moin, P. & You, D. 2010 Grid-independent large-eddy simulation using explicit filtering. *Phys. Fluids* **22**, 105103.

Bradshaw, P. 1987 Turbulent secondary flows. *Annu. Rev. Fluid Mech.* **19**, 53–74.

Brundrett, E. & Baines, W. D. 1964 The production and diffusion of vorticity in duct flow. *J. Fluid Mech.* **19**, 375–394.

Clark, R. A., Ferziger, J. H. & Reynolds, W. C. 1979 Evaluation of subgrid-scale models using an accurately simulated turbulent flow. *J. Fluid Mech.* **91**, 1–16.

Durbin, P. & Pettersson-Reif, B. A. 2010 *Statistical modeling for turbulent flow, 2nd ed*. Wiley and Sons.

Gavrilakis, S. 1992 Numerical simulation of low-Reynolds-number turbulent flow through a straight square duct. *J. Fluid Mech.* **244**, 101–129.

Germano, M. 1986*a* Differential filters for the large eddy simulation of turbulent flows. *Phys. Fluids* **29**, 1755–1766.

Germano, M. 1986*b* Differential filters of elliptic type. *Phys. Fluids* **29**, 1757–1758.

Haselbacher, A. & Vasilyev, O. V. 2003 Commutative discrete filtering on unstructured grids based on least-squares techniques. *J. Comp. Phys.* **187**, 197–211.

Kolade, B. O. 2010 Experimental investigation of a three-dimensional separated diffuser. PhD thesis, Stanford University.

Marsden, A. L., Vasilyev, O. V. & Moin, P. 2002 Construction of commutative filters for LES on unstructured meshes. *J. Comp. Phys* **175**, 584–603.

Meneveau, C. & Katz, J. 2000 Scale-invariance and turbulence models for large-eddy simulation. *Annu. Rev. Fluid Mech.* **32**, 1–32.

Mullen, J. S. & Fischer, P. F. 1999 Filtering techniques for complex geometry fluid flows. *Comm. Num. Meth. Eng.* **15**, 9–18.

Stolz, S., Adams, N. & Kleiser, L. 2001 An approximate deconvolution model for large-eddy simulation with application to incompressible wall-bounded flows. *Phys. Fluids* **13**, 997–1015.

Vreman, A. W. 2004 The adjoint filter operator in large-eddy simulation of turbulent flow. *Phys. Fluids* **16**, 2012.

Vreman, B., Geurts, B. & Kuerten, H. 1997 Large eddy simulation of the turbulent mixing layer. *J. Fluid Mech.* **339**, 357–90.

Winckelmans, G. S., Wray, A. A., Vasilyev, O. V. & Jeanmart, H. 2001 Explicit-filtering large-eddy simulation using the tensor-diffusivity model supplemented by a dynamic Smagorinsky term. *Phys. Fluids* **13**, 1385–1403.

You, D., Bose, S. T. & Moin, P. 2010 Grid-independent large-eddy simulation of compressible turbulent flows using explicit filtering. *Proc. 2010 Ctr. Turb. Res. Summer Prog.* pp. 203–210.